JOURNAL OF MATERIALS SCIENCE 17 (1982) 1753–1764

Superconducting properties and microstructure of crystallized Hf–Nb–Si and Hf–V–Si amorphous alloys

A. INOUE, Y. TAKAHASHI*, C. SURYANARAYANA†, T. MASUMOTO
The Research Institute for Iron, Steel and Other Metals, Tohoku University, Sendai 980, Japan

Amorphous Hf–Nb–Si and Hf–V–Si alloys have been produced by rapidly quenching the melts using a melt-spinning technique. The silicon content in the amorphous alloys was limited to 14 to 20 at% and the niobium or vanadium content was limited to 0 to 45 at% and 0 to 35 at%, respectively. These amorphous alloys did not show any superconducting transition down to liquid helium temperature (4.2 K). However, a transition was detected above 4.2 K after inducing crystallization in these alloys by annealing at appropriate temperatures. The highest superconducting transition temperatures, T_c, attained were 8.9 K for the $Hf_{45}Nb_{40}Si_{15}$ alloy annealed for 1 h at 1273 K and 6.7 K for the $Hf_{50}V_{35}Si_{15}$ alloy annealed for 1 h at 1173 K. The upper critical magnetic field, H_{c2}, at 4.2 K and the critical current density, J_c, at zero applied field and 4.2 K were about 5.1×10^6 A m^{-1} (6.4 T) and more than 1×10^4 A cm^{-2} for the $Hf_{45}Nb_{40}Si_{15}$ alloy and more than 8.0×10^6 A m^{-1} (10 T) and 5×10^3 A cm^{-2} for the $Hf_{50}V_{35}Si_{15}$ alloy. Detailed transmission electron microscopic studies of the annealed structure of these amorphous alloys established that, after crystallization, these alloys contain a body-centred cubic β-Hf(Nb) solid solution and body-centred tetragonal Nb_3Si phases in the $Hf_{45}Nb_{40}Si_{15}$ alloy and hexagonal Hf_5Si_3, face-centred cubic HfV_2 and cubic V_3Si phases in the $Hf_{50}V_{35}Si_{15}$ alloy. Since Nb_3Si and Hf_5Si_3 are not superconducting above 4.2 K, it has been concluded that superconductivity in these crystallized alloys is due to the precipitation of β-Hf(Nb) solid solution in the Hf–Nb–Si alloys and to the precipitation of HfV_2 and V_3Si compounds in the Hf–V–Si alloys.

1. Introduction

With a view to finding amorphous superconductors which can be easily produced in a continuous ribbon form and yet possess good mechanical properties, we have studied the conditions for the formation of the amorphous phase in refractory metal-based alloys [1–8] along with a critical evaluation of their mechanical properties, crystallization behaviour and superconducting properties. In these investigations, it was found that, in spite of the high reactivity, high melting-point and heavy atomic weight of hafnium, it was possible to produce continuous amorphous ribbons in hafnium-based alloys. The present paper deals with the crystallization behaviour and the resultant superconducting properties of amorphous Hf–Nb–Si and Hf–V–Si ternary alloys. Reasons for choosing these two alloy systems are two-fold: firstly, the equilibrium phase diagrams of Hf–V and Hf–Nb binary alloys belong to typical eutectic and isomorphous types [9], and, hence, it is interesting to investigate the effect of the type of phase diagram on the crystallization behaviour of refractory-metal based amorphous alloys; secondly,

*Present address: Graduate School, Department of Metallurgy, Tohoku University, Japan.
†Permanent address: Department of Metallurgical Engineering, Banaras Hindu University, Varanasi 221005, India.

0022–2461/82/061753–12$03.94/0

it was expected that the C–15-type HfV_2 [10] and A–15-type V_3Si [11] and Nb_3Si [12] compounds with a high superconducting transition temperature, T_c, and upper critical magnetic field, H_{c2}, might precipitate in the alloys crystallized from the amorphous state.

2. Experimental details

Alloys of different compositions were melted under an argon atmosphere in an arc furnace on a water-cooled copper hearth with a non-consumable tungsten electrode. The starting materials were hafnium (95 wt% pure, containing 3.4 wt% Zr and 0.05 wt% Nb impurities), silicon (99.999 wt% pure) and vanadium (99.8 wt% pure) or niobium (99.5 wt% pure). The weight of the mixture melted in one run was about 30 g. The ingots were repeatedly turned over and remelted to ensure homogeneity of composition. The compositions of alloys reported are the nominal ones since the losses during melting were negligible.

Continuous ribbon specimens of about 1 mm width and 0.02 mm thickness were obtained by melt spinning under a protective argon atmosphere. Details of the apparatus have been described in [6, 13]. Typically, the amount of alloys melted in one run was about 5 g and the rotation speed of the copper roller (20 cm in diameter) was about 4000 rpm.

The as-quenched phases were identified by conventional X-ray diffraction and transmission electron microscopy techniques. The ribbons were classified amorphous when the X-ray intensity as a function of the diffraction angle showed a typical liquid-like structure. Samples for electron microscopy were electrolytically thinned in an electrolyte consisting of 95 parts methanol and 5 parts sulphuric acid, cooled to approximately 220 K. The crystallization temperature, T_x, and the activation energy for crystallization, ΔE, were evaluated in a differential thermal analyzer (DTA) and a differential scanning calorimeter (DSC) at various heating rates ranging from 5 to 80 K min^{-1}. The hardness of specimens was measured by a Vickers microhardness tester with a 100 g load. The ductile–brittle transition behaviour was examined on specimens annealed for 1 h at different temperatures in evacuated quartz capsules. Ductility was evaluated by measuring the radius-of-curvature at fracture in a simple bend test. Methods to evaluate the superconducting properties have been described in detail in [14].

3. Results

3.1. Formation range of amorphous phase

The composition range in which the homogeneous amorphous phase formed in the $Hf_{85-x}V_xSi_{15}$ and $Hf_{85-x}Nb_xSi_{15}$ ternary systems is shown in Fig. 1. It can be seen that the range is rather wide, extending from 0 to 37 at% V or 0 to 45 at% Nb. However, the silicon content is limited to the narrow range of 14 to 20 at%. Electron microscopy and X-ray diffraction techniques confirmed the amorphous nature of the as-quenched material. No evidence of crystalline inclusions was found by means of dark-field electron microscopy for the alloys within the composition ranges described above.

It has been predicted from theoretical kinetic considerations [15–18] and experiments [19–21] that the formation of the amorphous phase is closely related to the reduced glass temperature, T_g/T_m (where T_g is the glass transition temperature and T_m is the melting point), and the viscosity of the alloys; that is, the larger the T_g/T_m and the higher the viscosity in the supercooled liquid, the greater is the ease of formation of the amorphous phase. In fact, the composition range in which amorphous alloys are obtained by the liquid-quenching technique is very often located around a deep eutectic in the alloy phase diagram, where T_m is the lowest. Each of the equilibrium diagrams for Hf–Si [22], V–Si [23], Hf–V [9] and Nb–Si [9] binary systems features a eutectic reaction at the compositions $Hf_{90}Si_{10}$, $V_{87}Si_{13}$, $Hf_{57}V_{43}$ and $Nb_{82}Si_{18}$, with the eutectic temperatures at 2273, 2053, 1731 and 2216 K, respectively. The present amorphous-forming composition ranges appear to fall around the troughs of the eutectics in the Hf–Nb–Si and Hf–V–Si ternary systems. A similar behaviour was observed in Ti–(Nb or V)–Si [1] and Zr–(Nb or V)–Si [24] systems. The high tendency to form amorphous phases in alloys having compositions near a deep eutectic has been interpreted in terms of a com-

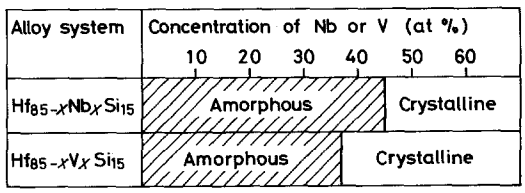

Figure 1 Composition range for the formation of an amorphous phase in the $Hf_{85-x}V_xSi_{15}$ and $Hf_{85-x}Nb_xSi_{15}$ alloys.

paratively large negative heat-of-formation of the liquid alloy [25]. Further, strong chemical interaction between hafnium and silicon and vanadium or niobium and silicon is expected to yield significantly high values of T_g and viscosity, thus promoting the formation of the amorphous phase.

3.2. Mechanical properties and thermal stability

All hafnium-based amorphous ribbons produced in the present investigation exhibited good bend ductility. For instance, the deformation structure of a $Hf_{45}Nb_{40}Si_{15}$ amorphous alloy bent completely by pressing around the edge of a thin razor blade is shown in Fig. 2. Although numerous deformation markings are seen near the bent edge, no cracks can be observed, even after such a severe deformation.

Vickers hardness, H_v, crystallization temperature, T_x, activation energy for crystallization, ΔE, and critical fracture temperature, T_f, were evaluated for the $Hf_{55}V_{30}Si_{15}$ and $Hf_{55}Nb_{30}Si_{15}$ alloys, and the results are presented in Table I. Here T_x is defined as the temperature corresponding to the start of the first exothermic peak of the differential thermal analysis (DTA) curve measured at a heating rate of 20 K min^{-1} and T_f is the temperature of ageing for 3.6 ksec which led to the fracture of alloys in a simple bend test. ΔE was calculated by measuring the position of the exothermic peak at different heating rates by the Kissinger method. The H_v, T_x and T_f values are, respectively, about 610 DPN, 930 K and 650 K for $Hf_{55}Nb_{30}Si_{15}$ and 640 DPN, 880 K and 600 K for $Hf_{55}V_{30}Si_{15}$. Also, ΔE is about 380 kJ mol^{-1} for the Hf–Nb–Si alloy and 365 kJ mol^{-1} for the Hf–V–Si alloy. The values of T_x, ΔE and T_f are higher for the Hf–Nb–Si alloy than for the Hf–V–Si alloy, indicating that the thermal stability is superior in the former alloy system.

3.3. Superconducting properties

3.3.1. Hf–Nb–Si amorphous alloys

Electrical resistance of $Hf_{55}Nb_{30}Si_{15}$ and $Hf_{45}Nb_{40}Si_{15}$ amorphous alloys was measured at low temperatures under no applied magnetic field in two conditions, both as-quenched and annealed for 1 h at various temperatures. T_c and ΔT_c values are plotted in Fig. 3 as a function of the annealing temperature. T_c is the temperature corresponding to $R/R_n = 0.5$, where R is the sample resistance and R_n is the resistance in the normal state. The transition width, ΔT_c, represented by a vertical bar in Fig. 3, represents the temperature interval between 0.1 and 0.9 of R/R_n. It is clear from Fig. 3 that the amorphous specimens remain in a normal state down to very low temperatures and are not superconducting in the temperature range investigated. This result is in contrast to the result that Ti–Nb–Si [14] and Zr–Nb–Si [24] amorphous alloys exhibit superconductivity at temperatures above about 3.0 K. Although the reason for such a difference is not clear at present, it may be due to the fact [26] that T_c of hafnium metal happens to be lower than that of titanium or zirconium. The $Hf_{55}Nb_{30}Si_{15}$ and $Hf_{45}Nb_{40}Si_{15}$ alloys annealed at temperatures above 973 K show a complete transition to the superconducting state above the liquid helium temperature. For both the specimens, T_c increases with increasing annealing temperature and appears to show maximum values at appropriate temperatures (the T_c value for $Hf_{45}Nb_{40}Si_{15}$ alloy continues to increase even after annealing at a temperature as high as 1273 K), as shown in Fig. 3. The highest T_c value attained is 8.9 K and is slightly lower than the highest value (10.0 K) [27] of crystalline Hf–Nb binary alloy. The lower T_c value for the alloy crystallized from the amorphous state appears to be caused by the limited annealing treatment and the dissolution of silicon in the superconducting phase.

The critical current density, J_c, was measured by a standard four-probe resistance method under an external applied magnetic field, H, in a liquid helium bath. As an example, Fig. 4 shows the critical current density, $J_c(H)$, as a function of H for $Hf_{45}Nb_{40}Si_{15}$ alloy annealed for 1 h at various

TABLE I Vickers hardness, H_v, crystallization temperature, T_x, the activation energy for crystallization, ΔE, and critical fracture temperature, T_f, for $Hf_{55}V_{30}Si_{15}$ and $Hf_{55}Nb_{30}Si_{15}$ amorphous alloys

Alloy system (at %)	Vickers hardness, H_v (DPN)	Crystallization temperature, T_x (K) (Rate = 20 K min^{-1})	Activation energy for crystallization, ΔE (kJ mol^{-1})	Critical fracture temperature, T_f (× 3.6 ksec K)
$Hf_{55}V_{30}Si_{15}$	640	882	365	≃ 600
$Hf_{55}Nb_{30}Si_{15}$	610	929	380	≃ 650

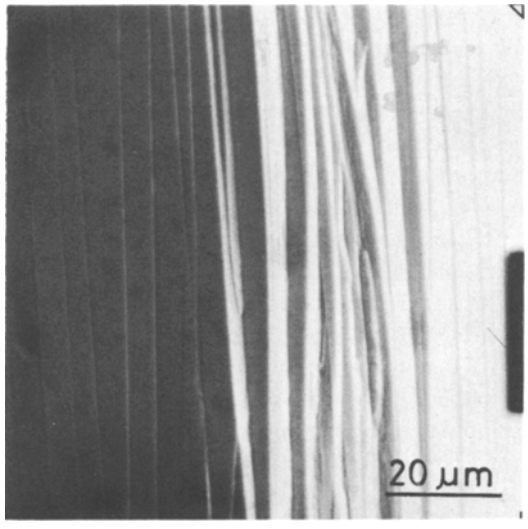

Figure 2 Scanning electron micrograph showing the deformation marking at the tip of $Hf_{45}Nb_{40}Si_{15}$ amorphous alloy bent through 180°.

temperatures. For $H = 0$, J_c increases with increasing annealing temperature and is more than about 1×10^4 A cm^{-2} for the alloy annealed at 1173 K. Similar temperature dependence is recognized for $J_c(H)$. For instance, $J_c(H)$ begins to decrease rapidly at about 2.6×10^6 A m^{-1} when annealed at 1023 K, while it remains unchanged up to about 4.2×10^6 A m^{-1} (5.3 T) and the specimen possesses a critical current density of about 6.3×10^3 A cm^{-2} at an applied field of 4.1×10^6 A m^{-1} (5.2 T). Fig. 5 shows the upper critical magnetic field, H_{c2}, of $Hf_{55}Nb_{30}Si_{15}$ and $Hf_{45}Nb_{40}Si_{15}$ alloys as a function of annealing temperature. Here, we define

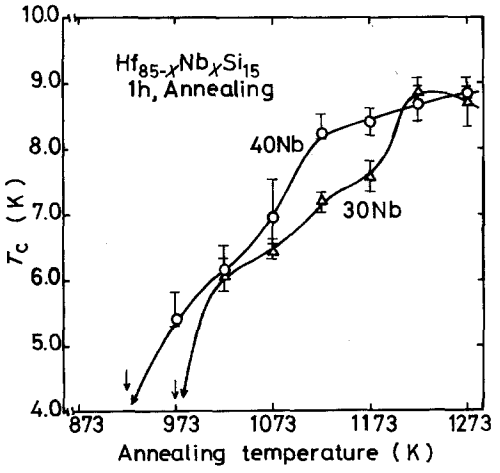

Figure 3 Change of superconducting transition temperature, T_c, for $Hf_{55}Nb_{30}Si_{15}$ and $Hf_{45}Nb_{40}Si_{15}$ amorphous alloys with annealing temperature. The vertical bars correspond to ΔT_c.

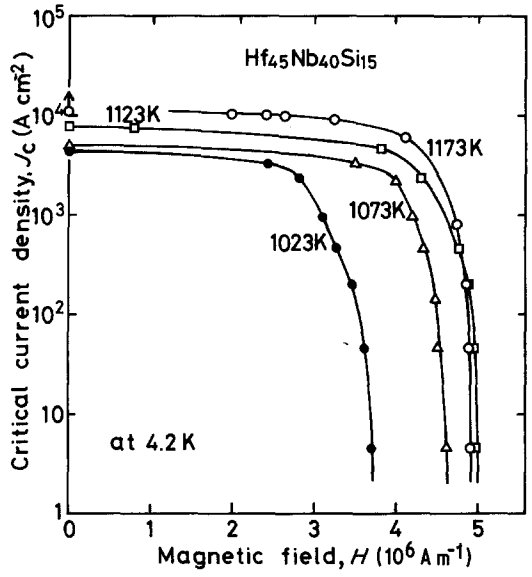

Figure 4 Critical current density, J_c, of $Hf_{45}Nb_{40}Si_{15}$ amorphous alloy annealed for 1 h at various temperatures as a function of magnetic field applied normal to the direction of current flow.

H_{c2} to be the applied magnetic field at which the resistance of the sample reaches half its normal value. The H_{c2} value increases with increasing annealing temperature, shows a maximum value at 1123 K, for example, about 4.7×10^6 A m^{-1} for $Hf_{55}Nb_{30}Si_{15}$ and 5.1×10^6 A m^{-1} for $Hf_{45}Nb_{40}Si_{15}$, and decreases slightly with further annealing. Such a temperature dependence is very similar to that of $J_c(H)$, but is significantly different from that of T_c, as evident from a comparison of Figs 3 to 5. The reason for such a difference will be discussed in a later section.

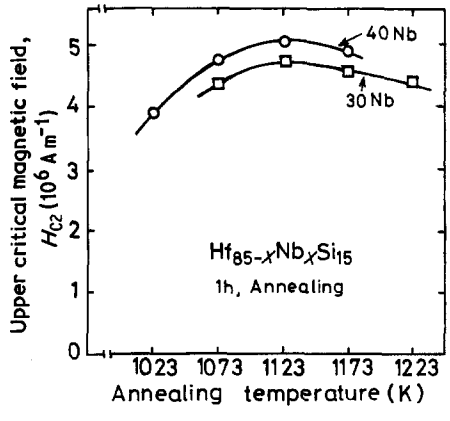

Figure 5 Change of upper critical magnetic field, H_{c2}, for $Hf_{55}Nb_{30}Si_{15}$ and $Hf_{45}Nb_{40}Si_{15}$ amorphous alloys with annealing temperature.

3.3.2. $Hf_{50}V_{35}Si_{15}$ amorphous alloy

The T_c value of the $Hf_{50}V_{35}Si_{15}$ amorphous alloy was measured for the as-quenched state and for two different annealed states, isochronally annealed for 1 h at various temperatures and isothermally annealed at 1223 K. The T_c and ΔT_c values thus obtained are plotted in Figs 6 and 7 as a function of the annealing temperature and annealing time. In Fig. 7, onset T_c is also plotted for comparison. The amorphous alloy remains in a normal state down to about 3.0 K, similar to the result of Ti–V–Si [28] and Zr–V–Si [29] amorphous alloys. However, annealing at temperatures exceeding 1123 K results in a complete transition to the superconducting state, but the annealing temperature and time are limited to narrow ranges; i.e., in the isochronal annealing for 1 h the temperature is in the range of 1123 to 1223 K and in the isothermal annealing at 1223 K the time is in the range of 15 to 80 min. Under these conditions, T_c increases with increasing annealing temperature or time, shows a maximum value at an appropriate temperature or time, and decreases later. The highest T_c value attained during the present limited annealing treatment is 6.7 K, as seen in Figs 6 and 7. The transition width, ΔT_c, is in the range of 0.3 to 2.4 K, although a systematic change with annealing treatment could not be observed.

Fig. 8 shows the critical current density, $J_c(H)$, of $Hf_{50}V_{35}Si_{15}$ alloy annealed for 1 h at 1223 K as a function of H, together with the data of T_c and H_{c2}. The highest $J_c(H)$ values of $Hf_{45}Nb_{40}Si_{15}$ alloy also are represented for comparison. For $H = 0$, J_c is of the order of 5×10^3 A cm^{-2} and this value remains almost unchanged for increasing H up to about 5×10^6 A m^{-1}. With further increase of the magnetic field, $J_c(H)$ begins to decrease significantly. However, as seen in Fig. 7, the J_c value of $Hf_{50}V_{35}Si_{15}$ alloy is of the order of 200 A cm^{-2} even at a high magnetic field of 7×10^6 A m^{-1}, and is much higher than that of $Hf_{45}Nb_{40}Si_{15}$ alloy at higher magnetic fields above about 5×10^6 A m^{-1}. Further, one can notice that the upper critical magnetic field, H_{c2} for $Hf_{50}V_{35}Si_{15}$ alloy appears to be higher than 8×10^6 A m^{-1} ($\simeq$ 10 T) when annealed at 1223 K.

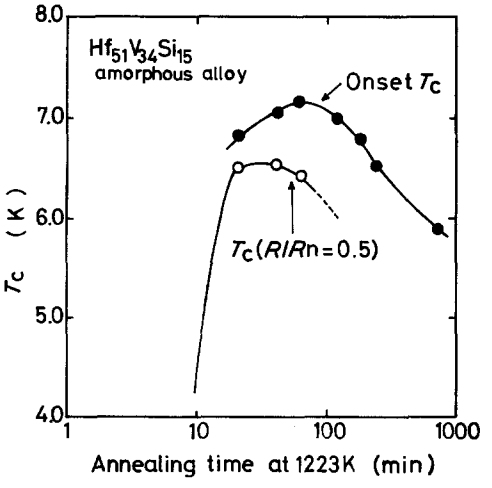

Figure 7 Changes of superconducting transition temperature, T_c, and onset transition temperature for $Hf_{50}V_{35}Si_{15}$ amorphous alloy with annealing time at 1223 K.

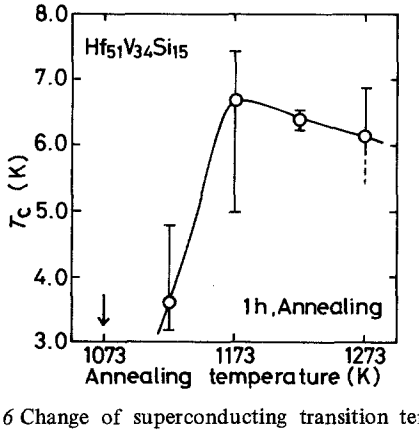

Figure 6 Change of superconducting transition temperature, T_c, for $Hf_{50}V_{35}Si_{15}$ amorphous alloy with annealing temperature. The vertical bars correspond to ΔT_c.

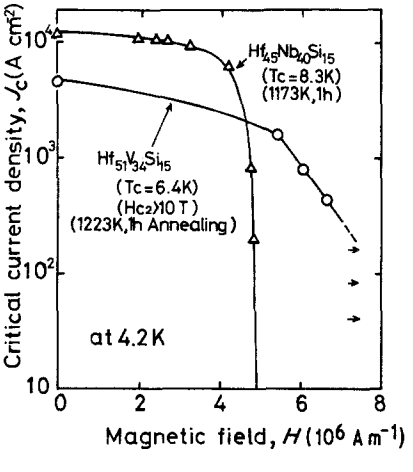

Figure 8 Critical current density, J_c, of $Hf_{50}V_{35}Si_{15}$ amorphous alloy annealed for 1 h at 1223 K, as a function of magnetic field applied normal to the direction of current flow. The data of $Hf_{45}Nb_{40}Si_{15}$ alloy annealed for 1 h at 1173 K are also represented.

3.4. Annealed structure

With a view to understanding the reason for the occurrence of superconductivity only when the amorphous Hf–Nb–Si and Hf–V–Si alloys were annealed, detailed transmission electron microscopic observations have been made on $Hf_{45}Nb_{40}Si_{15}$ and $Hf_{50}V_{35}Si_{15}$ alloys annealed for different periods at various temperatures, and the results are shown in Figs 9 to 12. Fig. 9 shows bright-field images and the corresponding selected-area diffraction patterns of the Hf–Nb–Si (Fig. 9a and b) and Hf–V–Si (Fig. 9c and d) alloys annealed for 30 min at 923 and 873 K, respectively. These temperatures are just below the temperatures where superconductivity begins to appear. Although a weak contrast can be seen all over the area in the highly magnified bright-field images (Fig. 9a and c), the diffraction patterns indicate that the amorphous structure of these alloys remains essentially unchanged even after such a high-temperature annealing.

Fig. 10 shows the electron micrographs and the selected-area diffraction patterns of the $Hf_{45}Nb_{40}Si_{15}$ alloy annealed for 1 h at 973 K (Fig. 10a and b) and 1123 K (Fig. 10c and d) corresponding to the temperatures where superconductivity begins to appear and the T_c value approaches the maximum value. As shown in the micrographs Fig. 10a and b, the microcrystals with an average size of 25 nm consist of β-Hf(Nb) with a body-centered cubic (bcc) structure and Nb_3Si-phase with a body-centred tetragonal (b c t) structure [30]. With increasing annealing temperature, the grain size of these phases increases gradually and is about 35 nm at 1123 K, as shown in Fig. 10c and d. We could not observe any other

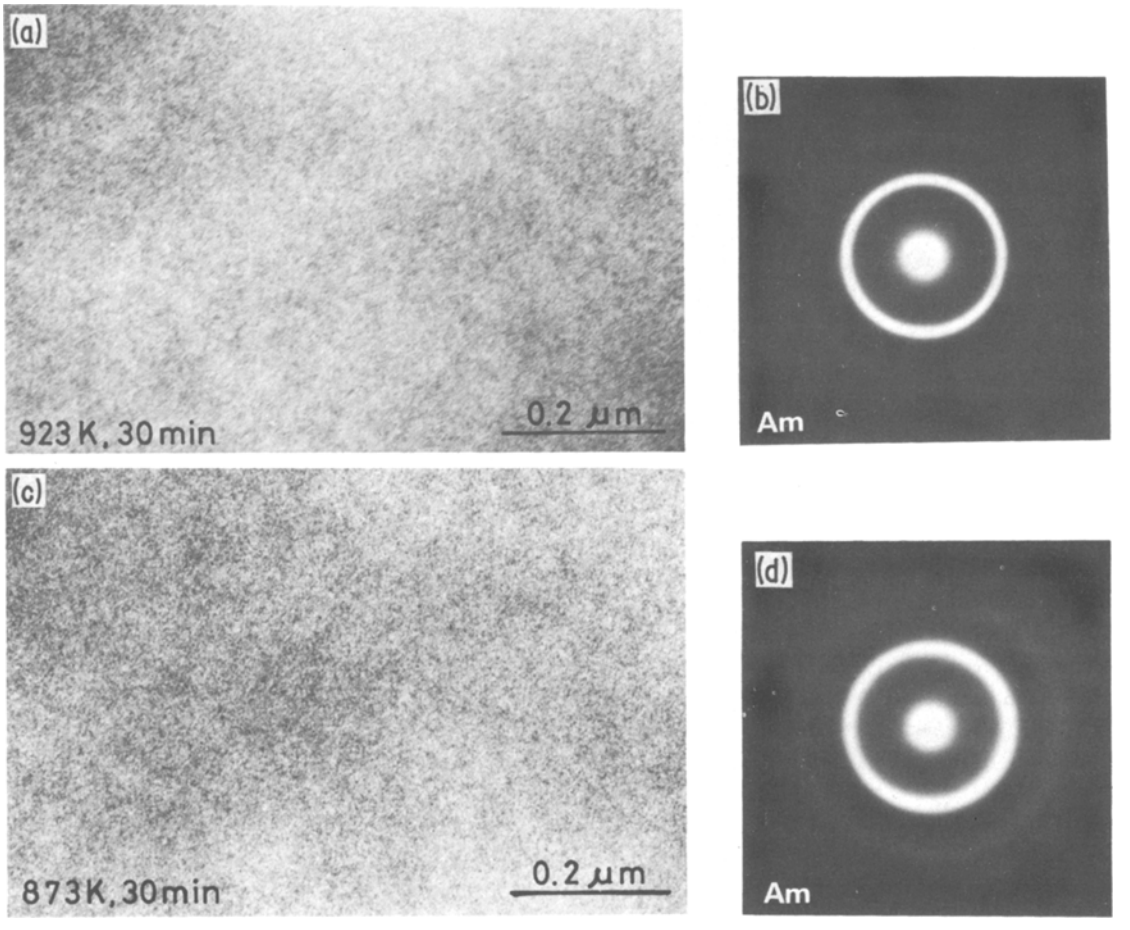

Figure 9 Transmission electron micrographs and selected-area diffraction patterns showing the annealed structures of (a and b) $Hf_{45}Nb_{40}Si_{15}$ alloy annealed for 30 min at 923 K and of (c and d) $Hf_{50}V_{35}Si_{15}$ alloy annealed for 30 min at 873 K. (b and d) show the amorphous nature of the alloys.

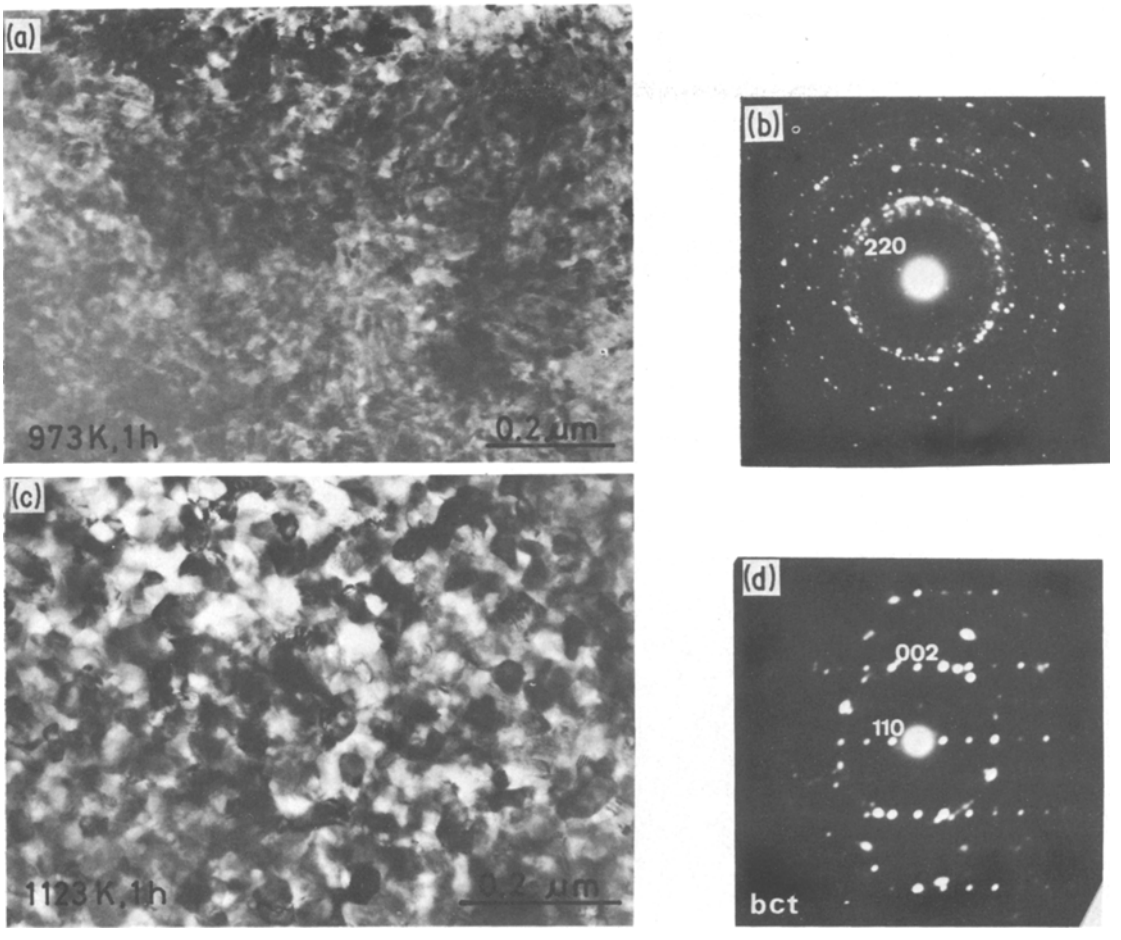

Figure 10 Transmission electron micrographs and selected-area diffraction patterns showing the crystallized structures of $Hf_{45}Nb_{40}Si_{15}$ alloy annealed for 1 h at (a and b) 973 K and at (c and d) 1123 K. (b and d) shows microcrystals to contain β-Hf(Nb) and Nb_3Si.

phase, even after annealing for 1 h at 1273 K. Hence, it is concluded that the $Hf_{45}Nb_{40}Si_{15}$ amorphous alloy crystallized from the amorphous state exhibits the duplex structure consisting of the β-Hf(Nb) and Nb_3Si phases.

Fig. 11 shows the microstructures of the $Hf_{50}V_{35}Si_{15}$ amorphous alloy annealed for 1 h at 1223 K and 1273 K. It has been shown in Fig. 6 that these annealing treatments result in the appearance of superconductivity. The average size of the crystallite is about 45 nm at 1223 K and 65 nm at 1273 K. As identified in Fig. 12, these crystalline phases are (i) Hf_5Si_3 with a hexagonal structure [30], (ii) HfV_2 with a face-centred cubic (f c c) structure [30] and (iii) V_3Si with a cubic structure [30]. It is very important to note that the crystallization of the Hf–V–Si amorphous phase leads to the precipitation of superconducting HfV_2 and V_3Si compounds, even though the amount of these phases appears to be rather small.

4. Discussion

4.1. Relation between superconductivity and annealed structures

Detailed and careful transmission electron microscopic observations have revealed that the specimens showing the superconducting transition consist of a mixture of the b c c β-Hf(Nb) solid solution and the b c t Nb_3Si-phase in the $Hf_{45}Nb_{40}Si_{15}$ alloy and a mixture of hexagonal Hf_5Si_3-phase, f c c HfV_2-phase and cubic V_3Si-phase in the $Hf_{50}V_{35}Si_{15}$ alloy. The b c t Nb_3Si [31] and the hexagonal Hf_5Si_3 [32] compounds have been shown to be non-superconducting above 4.2 K. Hence, it is concluded that superconduc-

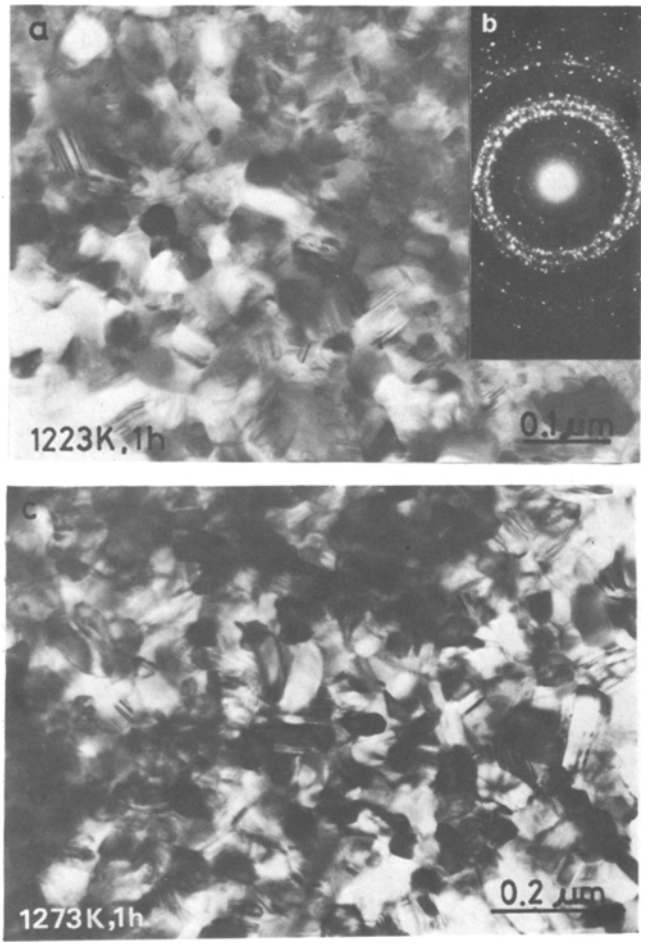

Figure 11 Transmission electron micrographs and selected-area diffraction patterns showing the crystallized structures of $Hf_{50}V_{35}Si_{15}$ alloy annealed for 1 h at (a and b) 1223 K and at (c) 1273 K.

tivity in these alloys is due to the precipitation of β-Hf(Nb) in Hf–Nb–Si alloys and HfV_2 and V_3Si compounds in Hf–V–Si alloy. The mechanism for the occurrence of superconductivity also seems to be different in these two alloy systems. While the major phase is β-Hf(Nb) solid solution in Hf–Nb–Si alloys, which is superconducting, the major phase is Hf_5Si_3 in Hf–V–Si alloys, which is non-superconducting. Hence, it appears reasonable to conclude that superconductivity in Hf–V–Si alloys is due to the proximity effect of HfV_2 and/or V_3Si phases. Thus, it is expected that Hf–V–Si alloys exhibit superconductivity only when these compounds are dispersed with a critical particle size and distance [33].

Silvert and Singh [34] have discussed theoretically the relationship between the size of superconducting particles and T_c, and have shown that the critical condition for the occurrence of superconductivity is given by $r_c > 2.965\ \xi_0$, where r_c is the radius of the superconducting particle and ξ_0 is the coherence length in the superconductor. ξ_0 has been reported to be 4.9 nm for V_3Si [35]. ξ_0 for HfV_2 appears to be of the same order, even though experimental data are not available. As a result, r_c is estimated to be about 15 nm. This value suggests that the radius of superconducting V_3Si or HfV_2 particles must be larger than 15 nm to achieve high T_c values by the proximity effect.

For the proximity effect in the case of "dirty limit"-type superconductor, as exemplified by V_3Si and HfV_2 compounds, the leak distance, K_n^{-1}, is given by the equation [33],

$$K_n^{-1} = (h v_n l_n / 6\pi k_B T)^{1/2}, \qquad (1)$$

where h is Planck's constant, v_n is the Fermi velocity of electrons in normal conducting theory, l_n is the mean free path of electrons in normal state and k_B is the Boltzmann constant. For achieving a high T_c value by the proximity effect, the superconducting V_3Si and HfV_2 particles must lie within the estimated K_n^{-1} value, in addition to

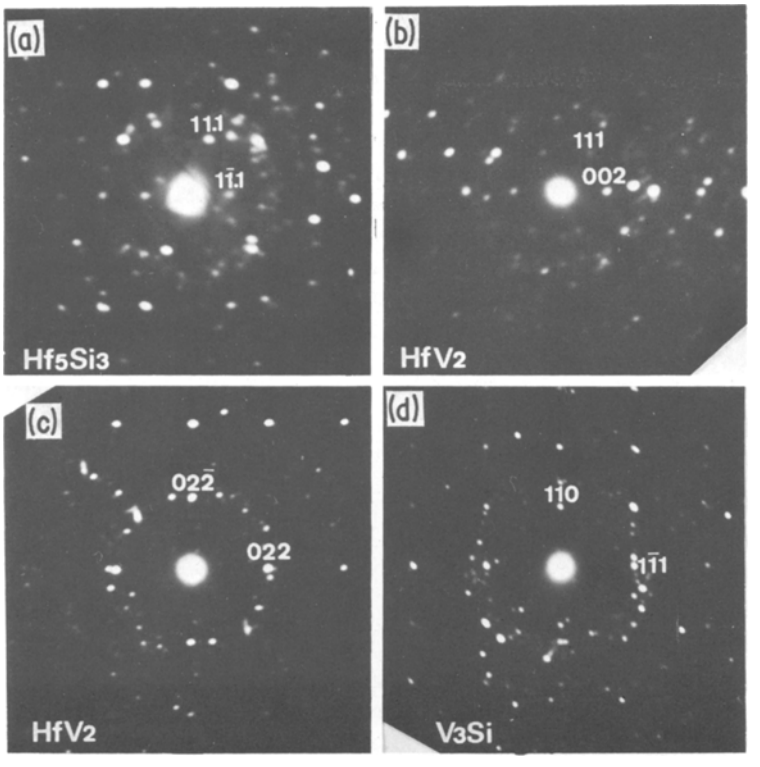

Figure 12 Selected-area electron diffraction patterns taken from $Hf_{50}V_{35}Si_{15}$ alloy annealed for 2 h at 1223 K.

satisfying the relation that $r_c > 2.965\ \xi_0$. Fig. 11 indicates that the average radius of the V_3Si or HfV_2 particles is about 23 to 33 nm, which is larger than the critical radius (15 nm) required for exhibiting superconductivity by the proximity effect. Further, considering the fact that this size increases further with subsequent annealing, it may be concluded that the critical condition for particle size is always satisfied, even on subsequent annealing. On the other hand, there is no information on the particle spacing of these superconducting phases because the identification of these compounds by the dark-field technique is made difficult by the extremely weak intensity of their reflection spots. However, the spacing between the particles is expected to increase considerably with increasing annealing temperature and/or time. As a result, the particle distance after long annealing exceeds the critical distance, K_n^{-1}, resulting in the disappearance of superconductivity due to the proximity effect. Therefore, in order to achieve a higher T_c value by the proximity effect for the present alloy systems, it seems essential to increase the amount of precipitated V_3Si and HfV_2 compounds by suitable alloy design.

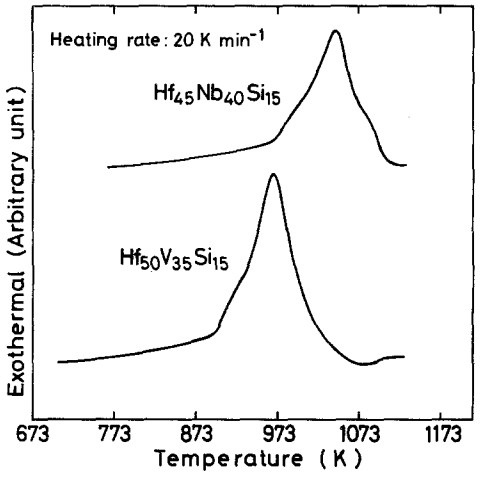

Figure 13 Differential thermal analysis curve of $Hf_{45}Nb_{40}Si_{15}$ and $Hf_{50}V_{35}Si_{15}$ amorphous alloys.

4.2. Temperature dependence of T_c and H_{c2}

It is well known that the value of J_c depends largely on the microstructure: on the density of precipitates, dislocations, grain boundaries and other defects which can serve as pinning centres. Hence, the temperature dependence of J_c is attributed to the microstructural change upon annealing. On the other hand, the temperature

dependence of T_c and H_{c2} is considered to be caused by a variation in the microscopic state of the superconducting phase. As shown in Figs 3 and 5, the T_c value of $Hf_{45}Nb_{40}Si_{15}$ alloy continues to increase with increasing annealing temperature in the temperature range below 1223 K, whereas H_{c2} shows a maximum value at 1123 K and tends to decrease with further annealing. According to McMillan [36], T_c is mainly dominated by the Debye temperature, θ_D, the electron–phonon coupling constant, λ, and the bare density of states at the Fermi level $N(0)$; the larger the values of θ_D, λ and $N(0)$, the higher is the value of T_c. Therefore, it may be stated that the increase in T_c with increasing annealing temperature is due to the increase of θ_D, λ and/or $N(0)$ through the concentration of niobium into the β-phase and/or the degradation of silicon in the β-phase. On the other hand, H_{c2} has been considered [37] to be dominated by the electrical resistivity in the normal state, ρ_n, electronic specific coefficient, γ, and T_c and there exists a relation that the larger the values of these parameters the higher is the value of H_{c2}. Since γ is proportional to $N(0)$ and λ [38], H_{c2} also has a proportional relation to ρ_n, $N(0)$, λ and T_c. Hence, it is inferred that the difference in the temperature dependences of T_c and H_{c2}, shown in Figs 3 and 5, is due to the change in ρ_n during annealing. Although the value of ρ_n is not measured in the present investigation, previous results [39, 40] suggest that its value is a maximum at the initial stage of crystallization where the crystalline phase begins to appear and that its value decreases significantly with growing crystalline particles. As a result, it may be stated that H_{c2} shows a maximum value in the temperature range where ρ_n remains relatively high and decreases with further annealing because of the significant lowering of ρ_n, even though the values of $N(0)$, λ and T_c increase.

4.3. Crystallization behaviour

In the present investigation we could not succeed in clarifying the initial stage of crystallization where the first crystallites begin to appear from the amorphous phase. Therefore, the crystallization process of the $Hf_{45}Nb_{40}Si_{15}$ and $Hf_{50}V_{35}Si_{15}$ amorphous alloys remains unknown, but we can have some insight into the process on the basis of the present results on annealed structures.

Failure to detect the initial stage suggests that the transformation from the amorphous to the crystalline phases occurs rapidly over a narrow temperature range, implying the simultaneous precipitation of β-Hf(Nb) and Nb_3Si in the Hf–Nb–Si alloy and Hf_5Si_3, HfV_2 and V_3Si in the Hf–V–Si alloy. This inference receives support from the observation that there exists only one exothermic peak in the DTA curves, as shown in Fig. 13. Therefore, the crystallization sequence in these alloys appears to follow the sequence:

(a) for the $Hf_{45}Nb_{40}Si_{15}$ alloy,

$$\text{Amorphous} \longrightarrow \beta\text{-Hf(Nb)} + Nb_3Si, \quad (2)$$

where β-Hf(Nb) is b c c with $a = 0.343$ nm and Nb_3Si is b c t with $a = 1.021$ nm and $c = 0.519$ nm; and

(b) for the $Hf_{50}V_{35}Si_{15}$ alloy,

$$\text{Amorphous} \longrightarrow Hf_5Si_3 + HfV_2 + V_3Si, \quad (3)$$

where Hf_5Si_3 is hexagonal with $a = 0.789$ nm and $c = 0.556$ nm, HfV_2 is f c c with $a = 0.739$ nm and V_3Si is cubic with $a = 0.472$ nm.

Further, one can notice that the type of precipitates is different for the $Hf_{45}Nb_{40}Si_{15}$ and $Hf_{50}V_{35}Si_{15}$ alloys. That is, the precipitates of the Hf–Nb–Si alloys consist of the β-Hf(Nb) solid solution and the b c t Nb_3Si-phase, in accordance with those of Ti–(V, Nb or Ta)–Si [28, 41, 42] and Zr–Nb–Si [24] amorphous alloys. On the other hand, the crystallized Hf–V–Si alloy contains only the Hf_5Si_3, HfV_2 and V_3Si phases, being the same as in the case of the Zr–V–Si [24] amorphous alloy. Judging from the fact [9] that the equilibrium phase diagram is of the complete miscibility type for Hf–Nb, Ti–(V, Nb or Ta) and Zr–Nb alloys and of the eutectic type for Hf–V and Zr–V alloys, it may be suggested that such a difference in the precipitates reflects the difference in the equilibrium phase diagram. From this result, the following empirical rule is deduced: if the appearance, upon crystallization of the amorphous phase, of intermetallic compounds consisting of major components is desired, one must select the alloy system of a eutectic type as exemplified by the Hf–V and Zr–V systems.

5. Conclusions

Amorphous alloys possessing high strength and good bend ductility were found in a wide composition range in the Hf–Nb–Si and Hf–V–Si systems. Continuous ribbons of about 1 mm width and about 0.02 mm thickness were produced using

a melt-spinning apparatus designed for refractory alloys. The amorphous phase could be obtained in alloys containing 0 to 45 at% Nb and 14 to 20 at% Si for the Hf–Nb–Si system and 0 to 37 at% V and 14 to 17 at% Si for the Hf–V–Si system. Vickers hardness and crystallization temperature were about 610 DPN and 930 K for $Hf_{55}Nb_{30}Si_{15}$ and 640 DPN and 880 K for $Hf_{55}V_{30}Si_{15}$. Further, these amorphous alloys are so ductile that no crack was found at the tip of a specimen bent through 180° around the edge of a thin razor blade. The specimens continued to be ductile when annealed for 1 h at temperatures below about 650 K for $Hf_{55}Nb_{30}Si_{15}$ and at temperatures below 600 K for $Hf_{55}V_{30}Si_{15}$.

The Hf–Nb–Si and Hf–V–Si alloys were not superconducting in the amorphous state, but showed a superconducting transition above liquid helium temperature (4.2 K) after crystallization. The highest transition temperatures, T_c, achieved were 8.9 K for $Hf_{45}Nb_{40}Si_{15}$ and 6.7 K for $Hf_{50}V_{35}Si_{15}$. In addition, the recorded values of the upper critical magnetic field, H_{c2}, at 4.2 K and the critical current density, J_c, at zero applied field and 4.2 K were of the order of 5.1×10^6 A m^{-1} (6.4 T) and above 1×10^4 A cm^{-2} for $Hf_{45}Nb_{40}Si_{15}$ and more than 8.0×10^6 A m^{-1} (10 T) and 5×10^3 A cm^{-2} for $Hf_{50}V_{35}Si_{15}$. The structure of the superconducting samples consisted of b c c β-Hf(Nb) and b c t Nb_3Si in the Hf–Nb–Si alloys and hexagonal Hf_5Si_3, f c c HfV_2 and cubic V_3Si in the Hf–V–Si alloys. Since Nb_3Si and Hf_5Si_3 are not superconducting above 4.2 K, it was concluded that superconductivity in these alloys resulted from the precipitation of β-Hf(Nb) solid solution in the Hf–Nb–Si alloys and precipitation of HfV_2 and V_3Si compounds in the Hf–V–Si alloys.

Acknowledgements

The authors are indebted to Mr A. Hoshi, Mr M. Kudo, Mr K. Sai and Mr Y. Ishikawa of the High Magnetic Field Laboratory of Tohoku University for extending facilities for critical magnetic field measurements.

References

1. A. INOUE, H. M. KIMURA, S. SAKAI and T. MASUMOTO, Proceedings of the Fourth International Conference on Titanium, Vol. 2, edited by H. Kimura and O. Izumi, Kyoto, Japan, May 1980 (The Metallurgical Society of AIME, New York 1980) p. 1137.
2. A. INOUE, Y. TAKAHASHI and T. MASUMOTO, *Sci. Rep. Res. Inst. Tohoku Univ.* **A-29** (1981) 296.
3. S. SAKAI, H. M. KIMURA, A. INOUE and T. MASUMOTO, unpublished work (1978).
4. T. MASUMOTO, A. INOUE, S. SAKAI, H. M. KIMURA and A. HOSHI, *Trans. Japan Inst. Met.* **21** (1980) 115.
5. A. INOUE, T. MASUMOTO, A. HOSHI and S. SAKAI, "Metallic Glasses, Science and Technology" Vol. 1, edited by C. Hargitai, I. Bakonyi and T. Kemeny (Central Research Institute for Physics, Budapest, Hungary, 1981) p. 433.
6. A. INOUE, S. SAKAI, H. M. KIMURA and T. MASUMOTO, *Trans. Japan Inst. Met.* **20** (1979) 255.
7. A. INOUE, S. SAKAI, H. M. KIMURA, T. MASUMOTO and A. HOSHI, *Scripta Metall.* **14** (1980) 235.
8. A. INOUE, Y. TAKAHASHI, K. AOKI, S. SAKAI and T. MASUMOTO, Proceedings of the 4th International Conference on Rapidly-quenched Metals, Sendai, Japan, August, 1981.
9. D. T. HAWKINS and R. HULTGREN, "Metals Handbook: Metallography, Structures and Phase Diagrams" Vol. 8 (American Society for Metals, Metals Park, Ohio, 1973).
10. D. DEW-HUGHES, *Cryogenics* **15** (1975) 435.
11. B. T. MATTHIAS, V. B. COMPTON and E. CORENZWIT, *J. Phys. Chem. Sol.* **1** (1961) 130.
12. C. SURYANARAYANA, W. K. WANG, H. IWASAKI, and T. MASUMOTO, *Sol. Stat. Comm.* **34** (1980) 861.
13. A. INOUE and T. MASUMOTO, *Sci. Rep. Res. Inst. Tohoku Univ. Supplement* **A-28** (1980) 165.
14. A. INOUE, H. M. KIMURA, T. MASUMOTO, C. SURYANARAYANA and A. HOSHI, *J. Appl. Phys.* **51** (1980) 5475.
15. M. H. COHEN and D. TURNBULL, *Nature* **189** (1961) 131.
16. D. TURNBALL, *Comtemp. Phys.* **10** (1969) 473.
17. D. R. UHLMANN, *J. Non-Cryst. Sol.* **7** (1972) 337.
18. H. A. DAVIES, Proceedings of the 3rd International Conference on Rapidly-quenched Metals, Vol. 1, edited by B. Cantor (The Metals Society, London, 1978) p. 1.
19. M. NAKA, Y. NISHI and T. MASUMOTO, Proceedings of the 3rd International Conference of Rapidly-quenched Metals, Brighton, July 1978, Vol. 1, edited by B. Cantor (The Metals Society, London, 1978) p. 231.
20. A. INOUE, T. IWADACHI, T. MINEMURA and T. MASUMOTO, *J. Japan Inst. Met.* **44** (1980) 245.
21. *Idem, Trans. Japan Inst. Met.* **22** (1981) 197.
22. R. P. ELLIOTT, "Constitution of Binary Alloys" First Supplement (McGraw-Hill Book Co., New York, 1965) p. 521.
23. C. J. SMITHELLS, "Metals Reference Book" 5th edition (Butterworths, London, 1976) p. 782.
24. A. INOUE, Y. TAKAHASHI and T. MASUMOTO, unpublished work (1981).
25. D. TURNBULL, *J. Physique-Colloq.* **35** (1974) 1.
26. T. H. GEBALLE, B. T. MATTHIAS, J. P. REMEIKA, A. M. CLOGSTON, V. B. COMPTON, J. P. MAITA and H. J. WILLIAMS, *Physics* **2** (1966) 293.

27. T. G. BERLINCOURT and R. R. HAKE, *Phys. Rev.* **131** (1963) 140.
28. A. INOUE, C. SURYANARAYANA, T. MASUMOTO and A. HOSHI, *Mater. Sci. Eng.* **47** (1981) 59.
29. A. INOUE, Y. TAKAHASHI and T. MASUMOTO, unpublished work (1980).
30. W. B. PEARSON, "A Handbook of Lattice Spacings and Structures of Metals and Alloys" (Pergamon Press, Oxford, 1967).
31. D. K. DEARDORFF, R. E. SIEMENS, P. A. ROMANS and R. A. McCUNE, *J. Less-Common Metals* **18** (1969) 11.
32. A. INOUE, Y. TAKAHASHI and T. MASUMOTO, unpublished work (1980).
33. G. DEUTSCHER and D. G. DE GENNES, "Superconductivity" Vol. 2, edited by R. Parks (Marcel Dekker, New York, 1969) p. 1005.
34. W. SILVERT and A. SINGH, *Phys. Rev. Lett.* **28** (1972) 222.
35. Y. MUTO, N. TOYOTA, K. NOTO, K. AKUTSU, M. ISHINO and T. FUKASE, *J. Low Temp. Phys.* **34** (1979) 617.
36. W. L. McMILLAN, *Phys. Rev.* **167** (1968) 331.
37. K. MAKI and T. TSUZUKI, *ibid.* **139** (1965) 868.
38. J. BARDEEN, L. N. COOPER and J. R. SCHRIEFFER, *ibid.* **108** (1957) 1175.
39. T. MASUMOTO, H. M. KIMURA, A. INOUE and Y. WASEDA, *Mater. Sci. Eng.* **23** (1976) 141.
40. T. MASUMOTO, A. INOUE and H. M. KIMURA, *J. Japan Inst. Met.* **41** (1977) 730.
41. A. INOUE, C. SURYANARAYANA, T. MASUMOTO and A. HOSHI, *Sci. Rep. Res. Inst. Tohoku Univ.* **A-28** (1980) 182.
42. A. INOUE, Y. TAKAHASHI, C. SURYANARAYANA, A. HOSHI and T. MASUMOTO, *J. Mater. Sci.* **16** (1981) 3077.

Received 30 September
and accepted 10 November 1981